PERGAMON

International Journal of Solids and Structures 38 (2001) 127–141

INTERNATIONAL JOURNAL OF SOLIDS and STRUCTURES

www.elsevier.com/locate/ijsolstr

Finite element analysis of damage evolution in Al/SiC composite laminates under cyclic thermomechanical loadings

H. Ismar, F. Schröter *, F. Streicher

Lehrstuhl für Technische Mechanik, Universität des Saarlandes, Postfach 15 11 50, D-66041 Saarbrücken, Germany

Received 19 July 1999

Abstract

In the current study, the nonlinear finite element method is used to formulate a micromechanical model of an aluminium alloy reinforced bidirectionally with high-modulus SiC fibres. Therewith, comprehensive numerical investigations of the thermomechanical cyclic behaviour of the laminate are possible.

Primarily, the geometrical model of the laminate is presented from which a three-dimensional unit cell can be deduced which is the starting point of further investigations. Subsequently, special emphasis is placed on the inelastic deformation behaviour of the metal matrix because of its significant influence on the composite behaviour. Therefore, a model which not only takes into account the coupling between viscoplasticity and damage but also allows an improved material description of the elastic–inelastic transition range by using the transition flow potential is recommended. Furthermore, thermal residual stresses induced by the manufacturing process have to be considered in the model.

At first, the cyclic mechanical behaviour of the laminate at a constant temperature is investigated at various strain amplitudes by closely analysing the evolution of the macroscopic hysteresis loops and the microscopic damage growth in the course of the cycles. Superimposing a cyclic thermal load to the mechanical load strongly influences the behaviour of the composite, whereby the phasing between the mechanical load and the temperature has a significant impact.

Keywords: Fibre-reinforced composite materials; Cyclic loading; Viscoplastic material; Damage; Finite elements

1. Introduction

With metal matrix composites (MMCs), materials science offers high-performance materials suitable for many weight-saving applications. This class of materials is especially attractive for structural applications because of its high strength-to-weight and stiffness-to-weight ratios even at elevated temperatures.

However, to submit an efficient employment and to take advantage of the entire application potential, the complex mechanical behaviour of MMCs has to be understood. Furthermore, the fact that the

* Corresponding author. Tel.: +49-681-3022157; fax: +49-681-3023992.
E-mail address: f.schroeter@rz.uni-sb.de (F. Schröter).

0020-7683/00/$ - see front matter
PII: S0020-7683(00)00032-9

deformation and failure mechanisms of MMCs are much more sophisticated under cyclic mechanical loadings than under purely monotonic loadings cannot be ignored.

However, in many typical applications, MMCs are subjected to a cyclic mechanical loading along with a superimposed variation in temperature. This type of loading condition is referred to as thermomechanical fatigue (TMF) and can be regarded as one of the most severe types because the significant difference in the coefficient of thermal expansion between the matrix and the fibre (Mall and Schubbe, 1994) causes high internal stresses raising irreversible deformation and failure mechanisms in the composite. Therefore, this type of loading is especially investigated in the current study.

The cost- and time-intensive experimental investigations of MMCs can be supported by micromechanical analyses. In contrast to the analytical models (Aboudi, 1982; Dvorak and Bahei-El-Din, 1982), computational methods such as the finite element method in combination with the unit cell approach allow a coverage of complex loading conditions and the inclusion of sophisticated material models which are able to describe the variety of different material effects. In order to predict accurately the time- and temperature-dependent properties of the composite, the constituents have to be modelled as exactly as possible. Therefore, a comprehensive unified viscoplastic constitutive theory extending Chaboche's model (Chaboche, 1977), which is one of the most precise constitutive models especially for metallic materials (Lion, 1994), is proposed. This theory also takes into account damage processes by using a continuum approach to damage mechanics (Lemaitre, 1985; Chaboche, 1988a,b).

Many numerical analyses have been carried out using a unit cell micromechanical model to compute the mechanical or thermomechanical behaviour of composites reinforced by continuous unidirectional fibres or short discontinuous fibres. To date, only a few researchers have examined the properties of multidirectionally reinforced MMCs. The current study focuses on a cross-ply laminate whose numerical investigation necessitates a three-dimensional model. Bigelow (1992) calculated thermal residual stresses in a SiC/Ti [0/90] laminate. For the same material, Nicholas et al. (1993) analysed the influence of a thermomechanical cyclic loading on the fatigue behaviour of the composite. Sherwood and Quimby (1995) used viscoplastic constitutive equations based on the theory of Bodner and Partom to investigate the damage growth in titanium-based metal matrix composites.

Because all previous analyses of cross-ply laminates known are based on titanium matrix composites, the current study focuses on the thermomechanical behaviour of aluminium bidirectionally reinforced with SiC fibres. Thus, it assists in addressing the lack of information of this uncertain class of materials.

2. Finite element model of the cross-ply laminate

To facilitate an analysis of the laminate by the finite element method, an idealisation of the fibre arrangement has to be introduced. Here an antisymmetric cross-ply laminate with the stacking sequence [0/90] is considered. The underlying idealisation in the form of a periodisation is presented in the upper part of Fig. 1 and is based on the subsequent geometrical assumptions:

- Fibres of straight cylinders are formed with circular cross-sections of the diameter $D_f = 2R_f$.
- All fibres possess identical geometry and are homogeneous.
- Fibres are infinitely long, i.e. the ratio of diameter D_f to length L_f is very small.
- Fibres are arranged parallely and unidirectionally in one ply with a distance between neighbouring fibre centrelines of $2A$.
- Two neighbouring plies are twisted around 90° to each other with a distance between adjoining crossed fibres of $2B$.
- Assuming a very thick laminate, border influences can be neglected.

From the geometric parameters R_f, A and B, the fibre volume fraction can be easily determined:

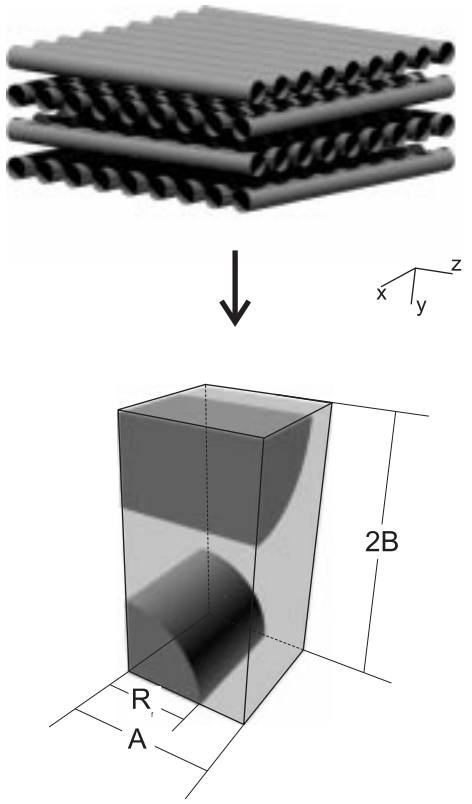

Fig. 1. Idealised fibre arrangement and resulting unit cell.

$$V_f = \frac{\pi}{4}\frac{R_f^2}{AB}. \tag{1}$$

By considering the symmetry of this fibre arrangement, the smallest three-dimensional representative part, the unit cell, is obtained. The lower part of Fig. 1 shows this extracted unit cell which is the basis for a finite element mesh of 780 8-noded brick elements and 912 nodes and which was created using the MENTAT preprocessor. Convergence studies with finer meshes and higher-order elements proved that this subdivision allows good results under acceptable computing times.

The macroscopic response of the laminate is decisively influenced by the inelastic deformation behaviour of the metallic matrix (Sherwood and Quimby, 1995). Therefore, viscoplastic constitutive equations with coupled damage are employed to describe the matrix. This model also allows an excellent representation of the elastic–inelastic material behaviour especially under cyclic loads as it comprehends ductile damage beginning with strong inelastic deformation. For the current study, this constitutive model was implemented into the finite element package MARC in the form of a user-supplied material model.

In contrast, the ceramic fibres are supposed to deform purely elastically in the applied temperature and load range. Fibres and metallic matrix are assumed to be perfectly bounded, so that no debonding occurs at the interface between the two constituents. This assumption is in agreement with experimental results of Flom and Arsenault (1986) who found the bonding between aluminium and silicon carbide to be very strong. Furthermore, interface stresses are limited by the relatively low stress level in the aluminium matrix, so that the interface does not show any debonding even for loads normal to the fibre axis.

3. Coupled viscoplastic-damage material model

The constitutive equations of metallic materials should take into account the most important effects of inelastic deformation such as the increase of the yield stress with rising deformation, time dependency, the Bauschinger effect (the premature inelastic deformation after a change of the loading direction) and the hysteresis loops under cyclic loading conditions. Therefore, an extended version of the unified viscoplastic material model of Chaboche (1977) was used to describe the metallic matrix in the composite. By expanding this model with the transition flow potential (TFP), a constitutive theory is obtained which is also able to describe changing yield surface geometry and accompanying inelastic volume changes as they were observed by Ismar et al. (1990) at the beginning of inelastic deformation after a purely elastic loading period.

Additionally, ductile damage caused by strong inelastic deformation influences the mechanical behaviour of the metallic matrix and, therefore, has to be considered too. Damage in metals due to inelastic deformation can be studied using different models (Bonora et al., 1994). By simplifying, these models can be grouped into two sets. Models based on an indirect damage variable use an additional variable calculated by the current value of stress, strain or energy (Rice et al., 1969; McClintock, 1968). On the contrary, the continuum damage mechanics (CDM) includes theories in which damage is represented by one or several constitutive thermodynamic variables calculated by coupling them with stresses and strains. This approach was also employed in the current study.

Damage is introduced here by Kachanov's (1958) concept of effective stress

$$\tilde{\sigma}_{ij} = \frac{\sigma_{ij}}{1-\omega}, \tag{2}$$

where σ_{ij} are the components of the stress tensor and ω, a scalar variable of damage caused by rising microdefects as microcracks and microvoids. This scalar definition of damage implies the similarity of the mechanical response under compression and tension. However, as Hansen and Schreyer (1995) stated, the microdefects may partially close in compression leading to a deactivated damage status. Therefore, an active damage variable

$$\tilde{\omega} = \omega\left[\Theta(I_1^\sigma) + H(1-\Theta(I_1^\sigma))\right] = \begin{cases} \omega, & I_1^\sigma \geqslant 0, \\ H\omega, & I_1^\sigma < 0, \end{cases} \tag{3}$$

is considered here. $\Theta(\cdot)$ represents Heaviside's function, $I_1^\sigma = \sigma_{ii}$, the first invariant of the stress tensor and H, the so-called microcrack closure parameter (Lemaitre, 1992) with $0 \leqslant H \leqslant 1$.

Assuming small deformations, the total strain rate tensor $\dot{\varepsilon}_{ij}$ is a linear superposition of an elastic $\dot{\varepsilon}^{\mathrm{e}}_{ij}$, a thermal $\dot{\varepsilon}^{\mathrm{t}}_{ij}$ and an inelastic component $\dot{\varepsilon}^{\mathrm{i}}_{ij}$, i.e.

$$\dot{\varepsilon}_{ij} = \dot{\varepsilon}^{\mathrm{e}}_{ij} + \dot{\varepsilon}^{\mathrm{t}}_{ij} + \dot{\varepsilon}^{\mathrm{i}}_{ij}. \tag{4}$$

Considering the principle of strain equivalence (Lemaitre, 1992), which states that any strain constitutive equation for the damaged material is derived by substituting the stress by the effective stress in the equations of the virgin material, the law of linear thermoelasticity of the damaged material is obtained:

$$\dot{\varepsilon}^{\mathrm{e}}_{ij} + \dot{\varepsilon}^{\mathrm{t}}_{ij} = \frac{1}{E(1-\omega)}\left((1+\upsilon)\dot{\sigma}_{ij} - \upsilon\dot{\sigma}_{kk}\delta_{ij}\right) + \alpha^{\mathrm{t}}\dot{T}\delta_{ij} \tag{5}$$

with the rate of stress $\dot{\sigma}_{ij}$ (which is not a frame invariant), the temperature T and the temperature-dependent material parameters Young's modulus $E = E(T)$, Poisson's ratio $\upsilon = \upsilon(T)$ and tangent coefficient of thermal expansion $\alpha^{\mathrm{t}} = \alpha^{\mathrm{t}}(T)$.

In order to couple damage constitutive equations also with the viscoplastic equations, an inelastic potential is defined in the effective stress space:

$$\Omega = \frac{K}{N+1}\left\langle \frac{\tilde{s}_v(\tilde{s}_{ij}) - r}{K} \right\rangle^{N+1} = \frac{K}{N+1}\left\langle \frac{\tilde{s}_o}{K} \right\rangle^{N+1}, \tag{6}$$

where K and N are material parameters, $\langle . \rangle$, the Mac Auley brackets and $\tilde{s}_{ij}$, the components of the effective active stress tensor,

$$\tilde{s}_{ij} = \tilde{\sigma}_{ij} - \sum_{k=1}^{m} x_{ij}^{k}, \tag{7}$$

which can be interpreted as the difference between the components of the effective stress tensor and several kinematic hardening variables x_{ij}^{k}. The effective active equivalent stress $\tilde{s}_v$ will be discussed below. The elastic domain (potential surface with $\Omega = 0$) is defined by the condition

$$\tilde{s}_v(\tilde{s}_{ij}) - r = \tilde{s}_o \leqslant 0. \tag{8}$$

In Eq. (8), r is the isotropic hardening and $\tilde{s}_o$, the effective overstress which describes a measure for the distance from the effective stress point to the corresponding point of the elastic domain.

Applying the kinetic equation, we receive the components of the inelastic strain rate,

$$\dot{\varepsilon}_{ij}^{i} = \frac{\partial \Omega}{\partial \tilde{s}_{ij}} = \underbrace{\left\langle \frac{\tilde{s}_o}{K} \right\rangle^{N}}_{\dot{\varepsilon}_v^{i}} \frac{\partial \tilde{s}_v}{\partial \tilde{s}_{ij}} \frac{\partial \Omega}{\partial \tilde{s}_v}, \tag{9}$$

where $\dot{\varepsilon}_v^{i}$ marks the equivalent inelastic strain rate.

Typically, the inelastic deformation of metals is described by using the v. Mises potential which is based on the hypothesis of inelastic incompressibility. As mentioned previously, recent investigations on certain materials have shown that inelastic volume changes occur at the beginning of inelastic deformation. Therefore, the viscoplastic model was improved by implementing the TFP formulated by Mahrenholtz and Ismar (1979). Thus, we receive for the equivalent effective active stress

$$\tilde{s}_v = \sqrt{\frac{\left(\chi I_1^{\tilde{s}}\right)^2 + 6 I_2^{\tilde{s}'}}{\chi^2 + 2}} \tag{10}$$

with the first invariant of an effective active stress $I_1^{\tilde{s}} = \tilde{s}_{ii}$ and the second invariant of an effective active stress deviator $I_2^{\tilde{s}'} = \frac{1}{2}\tilde{s}_{ij}'\tilde{s}_{ij}'$.

The internal variable χ can be interpreted as the ratio of small (r_1) to large (r_2) half axis of an ellipsoid of revolution-shaped potential surface. In the stress space, Fig. 2 compares a meridional section through the TFP for $\chi = 0.6$ with a section through the v. Mises potential which can be obtained from Eq. (10) by setting $\chi = 0$.

As is shown in Fries et al. (1997), the yield surface of the TFP changes its shape during the preceding inelastic deformation. This change in shape can be realised in the model by assuming χ as a function dependent on the inelastic strain of the respective load cycle $\varepsilon_{v,n}^{i}$

$$\dot{\chi} = -A_2 \chi \dot{\varepsilon}_{v,n}^{i} \tag{11}$$

with a material parameter A_2.

Beginning with a new inelastic deformation cycle after traversing the elastic domain, χ starts with the initial value

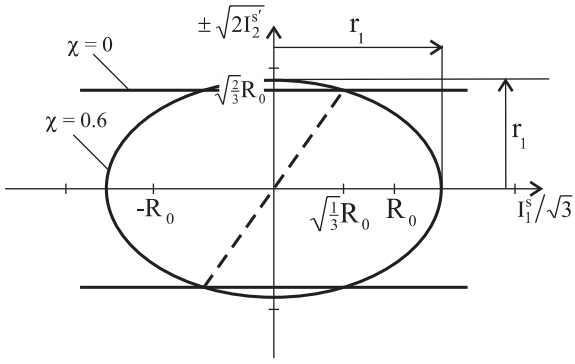

Fig. 2. Meridional section through the yield surface of the TFP ($\chi = 0.6$) and the v. Mises potential ($\chi = 0$).

$$\chi(\varepsilon^{\mathrm{i}}_{v,n} = 0) = A_1 \exp\left(-\left\langle \frac{y^n_{ij} \cdot \dot{\varepsilon}^{\mathrm{i}}_{ij}}{\dot{\varepsilon}^{\mathrm{i}}_{v}} \right\rangle \right), \tag{12}$$

where A_1 is a material parameter and y^n_{ij}, a reference tensor which is updated with the current value of the auxiliary tensor y_{ij} when unloading occurs.

This auxiliary tensor evolves according to

$$\dot{y}_{ij} = \chi^2(A_3\dot{\varepsilon}^{\mathrm{i}}_{ij} - A_4\dot{\varepsilon}^{\mathrm{i}}_{v}y_{ij}) \tag{13}$$

with the material parameters A_3 and A_4.

As an example, these evolution equations (11)–(13) are demonstrated in Fig. 3 for the case of purely monotonic loading. Then, χ tends to zero with increasing inelastic strain degenerating the yield surface to the v. Mises cylinder.

Moreover, the variables of kinematic and isotropic hardening have to be defined. A good representation of the cyclic hardening behaviour of metallic materials can be obtained by modifying the usual linear kinematic hardening rule (Prager's rule) with a recall term. Furthermore, thermal recovery effects appearing at an elevated temperature can be incorporated. Thus, we obtained

$$\dot{x}^k_{ij} = \frac{(\chi^2+2)}{3} C^k(1-\tilde{\omega})\dot{\varepsilon}^{\mathrm{i}}_{ij} - \Gamma^k(1-\tilde{\omega})\dot{\varepsilon}^{\mathrm{i}}_{v}x^k_{ij} - \underbrace{\Gamma^{rk}\left(x^k_v\right)^{M^k-1}x^k_{ij}}_{\text{thermal recovery}}. \tag{14}$$

Herein C^k, Γ^k, Γ^{rk} and M^k are material constants and x^k_v is an equivalent value of the kinematic hardening tensor. As the index k denotes several kinematic hardening terms of the same type are superposed allowing a greater flexibility in the adaptation of the kinematic hardening on the material behaviour.

The hardening model is complemented by the isotropic hardening r causing an expansion of the yield surface. This evolves according to

$$\dot{r} = B(Q-r)(1-\tilde{\omega})\dot{\varepsilon}^{\mathrm{i}}_{v} - \underbrace{\Gamma^r(r-Q^r)}_{\text{thermal recovery}} \tag{15}$$

starting from the initial value $r(\varepsilon^{\mathrm{i}}_v = 0) = R_0$. B, Q, Q^r and Γ^r are material parameters.

Finally, the growth of damage is given by (Lemaitre, 1992)

$$\dot{\omega} = \frac{g}{S}\dot{\varepsilon}^{\mathrm{i}}_{v}\Theta(\varepsilon^{\mathrm{i}}_v - \varepsilon^{\mathrm{i}}_{v0}), \tag{16}$$

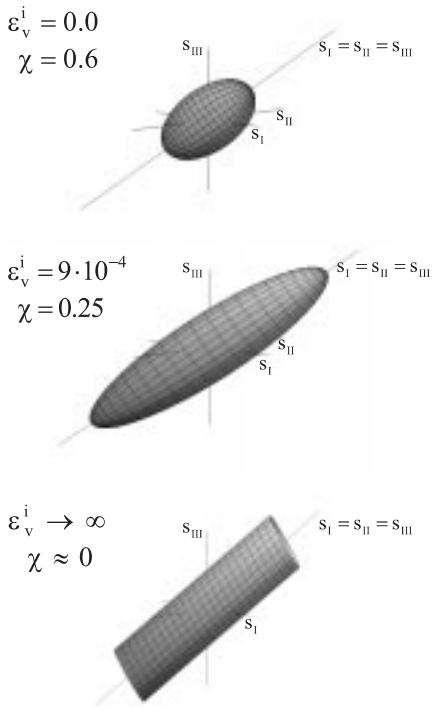

Fig. 3. TFP in the mean active stress space under monotonic loading.

where ε_{v0}^i is the equivalent inelastic strain below which no damage occurs, S, a material parameter and g, the damage energy release rate

$$g = \frac{1}{2E(1-\tilde{\omega})}\left((1+v)I_2^{\sigma'} + \frac{1-2v}{3}\left(I_1^{\sigma}\right)^2\right). \tag{17}$$

Therewith, the sophisticated material law is completed.

4. Investigated composite material

The composite laminate investigated in this study is a cross-ply reinforced SiC/Al with a fibre volume fraction of $V_f = 32\%$. Under the condition of identical distances between neighbouring parallel fibres in one ply and between neighbouring crossed fibres in adjoining plies, which means the equality of the geometric parameters A and B in Fig. 1, and assuming a fibre diameter of $D_f = 140$ μm this fibre volume fraction results in a ply thickness of 219 μm. As our comparing simulations performed before have shown, minor discrepancies between the geometric parameters do not seriously influence the macroscopic behaviour of the composite.

The matrix of the laminate is described by a cold-aged AlMgSi1 alloy (EN AW-6082) whose elastic, thermal and viscoplastic parameters were determined on monolithic samples at our laboratories (Ismar and Penth, 1998). Three distinct sets of parameters at 20°C, 100°C and 200°C were used because of the strong temperature dependency of the material parameters. Values between these sampling points were obtained by linear interpolation. The damage parameters were adopted from Lemaitre (1992).

As mentioned before, the isotropic and homogeneous fibres deform purely elastically. In order to model the composite behaviour as realistically as possible, the fact cannot be neglected that because of the large difference of the coefficients of thermal expansion between the ceramic fibre and the metallic matrix, residual stresses develop during the fabrication process in which the composite passes through several temperature regions. Additionally, this induced residual stress state can also cause inelastic deformation processes which significantly influence the mechanical behaviour of the laminate.

Therefore, in all subsequent simulations, a cooling process from the stress-free temperature of 200°C to 20°C with a cooling rate of 4°C s^{-1} followed by a hold time of 400 s is considered. The residual stress and deformation state due to the cooling process are more exactly specified by Ismar and Schröter (1999).

5. Results and discussion

5.1. Cyclic mechanical load

Primarily, the behaviour of the laminate was examined under cyclic mechanical loads oriented parallel to one of the two fibres. Various strain-controlled loadings with macroscopic strain amplitudes $\Delta\varepsilon_{mac}$ of 0.1%, 0.15% and 0.2% were performed over 40 cycles at a loading rate of $\dot{\varepsilon}_{mac} = 10^{-5}$ s^{-1}. In all cases, the temperature was kept constant at 100°C.

Fig. 4 compares the macroscopic stress–strain hysteresis loops of the three different strain amplitudes for the first, fifth and 40th loading cycles, respectively. Conspicuously, the asymmetric shape of these hysteresis loops provoked by the thermal residual stresses after thermal preloading can be observed. At each loading condition, the absolute value of the minimum macroscopic stress is higher than the value of the corresponding maximum macroscopic stress. This asymmetry increases with increasing strain amplitudes because the absolute value of the minimum stress grows faster than the maximum stress when external strain amplitude increases.

Moreover, a decrease in the maximum macroscopic stress and an increase in the absolute value of the minimum macroscopic stress in the course of the cycles is observed when loaded with a strain amplitude of

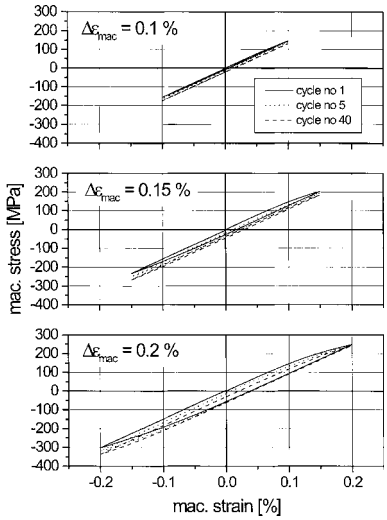

Fig. 4. Stress–strain cycles of the laminate under different strain amplitudes.

0.1% or 0.15%. Thereby, the decline of the maximum macroscopic stress is not as high as the increase of the absolute value of the minimum macroscopic stress.

Under the condition of $\Delta\varepsilon_{mac} = 0.2\%$, only a slight decrease of the maximum macroscopic stress can be recognised, whereas the absolute value of the minimum macroscopic stress still increases. Comparing the three different loops for a certain strain amplitude, the decrease of the maximum macroscopic stress and the increase of the absolute value of the minimum stress concentrate on the beginning cycles. Thus, especially for the strain amplitudes of 0.15% and 0.2%, it can be observed that the maximum and minimum stresses alter during the first five cycles almost as strongly as during the subsequent 35 cycles.

Fig. 4 also reveals fluctuations and a narrowing of the hysteresis in the course of the cycles. The effect of the shifting hysteresis (called ratchetting) is summarised in Fig. 5 using the magnitude of the remaining strain ε_m defined as the average of the macroscopic strain values of one loop at $\sigma_{mac} = 0$.

At all loadings, the hysteresis varies continuously but with declining rate to higher remaining strains. Providing a constant cycle number, an increase of the strain amplitude from 0.15% to 0.2% causes a smaller growth of the remaining strain than an increase of the strain amplitude from 0.1% to 0.15%. Special attention has to be directed to the relative incline of the remaining strain. Thus, under a strain amplitude of 0.1%, the remaining strain after 40 cycles is 4.3 times higher than that after the first cycle, whereas under strain amplitudes of 0.15% and 0.2%, only a hysteresis fluctuating after 40 cycles can be observed which is 2.7 resp. 1.7 times higher than the initial value.

Additionally, after finishing 40 cycles the loops have much more shift in the case of small external loadings because the slope at the end of the curve is by far the greatest at a loading amplitude of $\Delta\varepsilon_{mac} = 0.1\%$.

As already indicated in Fig. 4, an increasing narrowing of the hysteresis loops in the course of the cycles can also be detected. This phenomenon leads to a continuous decline of the deformation energy per cycle dissipated by inelastic-deformation mechanisms. Thus, Fig. 6 displays for the three investigated strain amplitudes the evolution of the inelastic work of deformation w^i normalized to the highest value w^i_{max} appearing at a strain amplitude of $\Delta\varepsilon_{mac} = 0.2\%$ in the first cycle in the course of loading.

Inelastic deformation still proceeds after 40 cycles – even under the condition of the smallest load amplitude of $\Delta\varepsilon_{mac} = 0.1\%$. Thereby, at $\Delta\varepsilon_{mac} = 0.1\%$, the inelastic work of deformation was lessened to 20%, at $\Delta\varepsilon_{mac} = 0.15$–32%, and at $\Delta\varepsilon_{mac} = 0.2$–53% of the respective maximum value. This reduction of variation indicates that the hysteresis width diminishes more slowly when the external load amplitude is raised.

Moreover, the different maximum values of the three loading cases have to be regarded. At a strain amplitude of 0.2% (0.15%), the maximum value of the inelastic work of deformation is 12.5 times (4.7

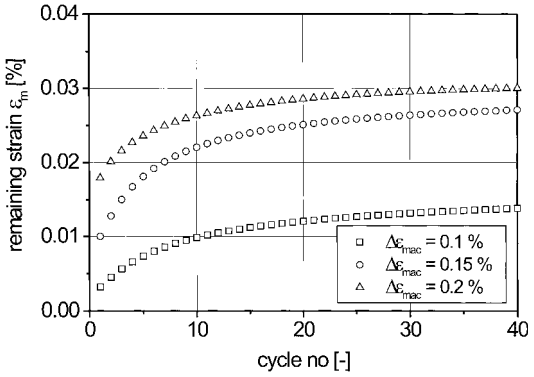

Fig. 5. Fluctuations of the hysteresis during the course of the cycles.

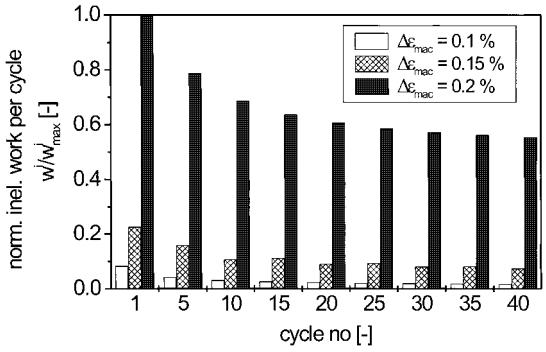

Fig. 6. Normalised inelastic work of deformation per cycle in the course of the cycles.

times) higher than the maximum value at a strain amplitude of 0.1%. Consequently, Fig. 6 clarifies the fact that the inelastic deformation extent strongly increases with increasing external strain amplitudes. Furthermore, the decline of the inelastic deformation extent in the course of the cycles is not as pronounced as at lower strain amplitudes.

Nevertheless, the metallic matrix still deforms inelastically after 40 cycles of the lowest investigated loading level of $\Delta\varepsilon_{mac} = 0.1\%$ denoting that no shake-down of the composite can be determined even at the lowest load level. On the other hand, the analysis of the loading with $\Delta\varepsilon_{mac} = 0.2\%$ proved that broad areas of the matrix were subjected to extensive inelastic deformation causing ductile damage in the highly strained matrix regions which can be interpreted by the nucleation and growth of microcavities.

Whereas, at the lower loadings, only little or no damage is detected within 40 cycles, Fig. 7 compares the damage distribution in the matrix at a loading of $\Delta\varepsilon_{mac} = 0.2\%$ after the fifth and the 40th loading cycle. After the fifth cycle, damage is strongly concentrated in the matrix area directly in front of the perpendicularly loaded fibre under approximately 50° to the external load indicated by the black arrow. Following

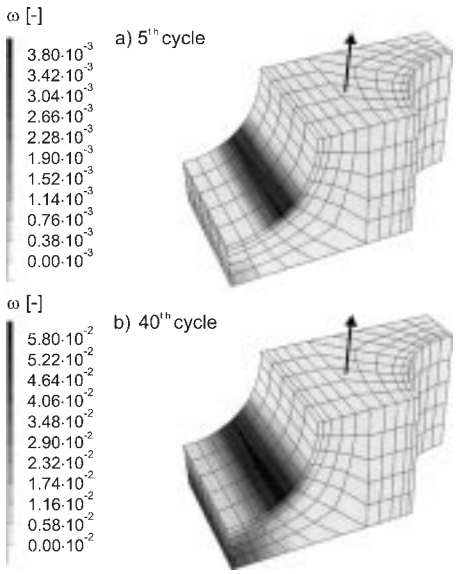

Fig. 7. Damage growth in the matrix during cyclic loading with $\Delta\varepsilon_{mac} = 0.2\%$.

an axial path parallel to this fibre through the highly damaged matrix region starting from a point lying in the front plane, which contains the minimum distance between crossed fibres, only a slight decrease in the amount of damage can be observed.

At the end of the 40th cycle, the maximum value of damage has strongly increased being more than 15 times higher than that after the fifth loading cycle. Obviously, the highly damaged area has enlarged circumferentially to the perpendicularly loaded fibre. Moreover, a region of great damage values has emerged in the area lying in the middle between parallely and perpendicularly loaded fibres. As opposed to the other strongly damaged region, the maximum is not situated directly in front of the fibre, because this region is characterised by negative mean stresses which hinder damage growth.

The results of the calculations – especially the distribution of inelastic deformation and accompanying damage in the transversely loaded ply – agree qualitatively well with the results of Bonora et al. (1994). Therefore, the computations can assist in understanding the complex deformation behaviour of this group of composites.

5.2. Thermomechanical cyclic loading

In many applications, metal–matrix composites are subjected simultaneously to varying mechanical and thermal loads. Thereby, the phasing between temperature and mechanical loads significantly influences the behaviour of the composite. Therefore, among the infinitely possible phasings, three different thermomechanical loading conditions will be examined for which Fig. 8 describes in each case one cycle of loading.

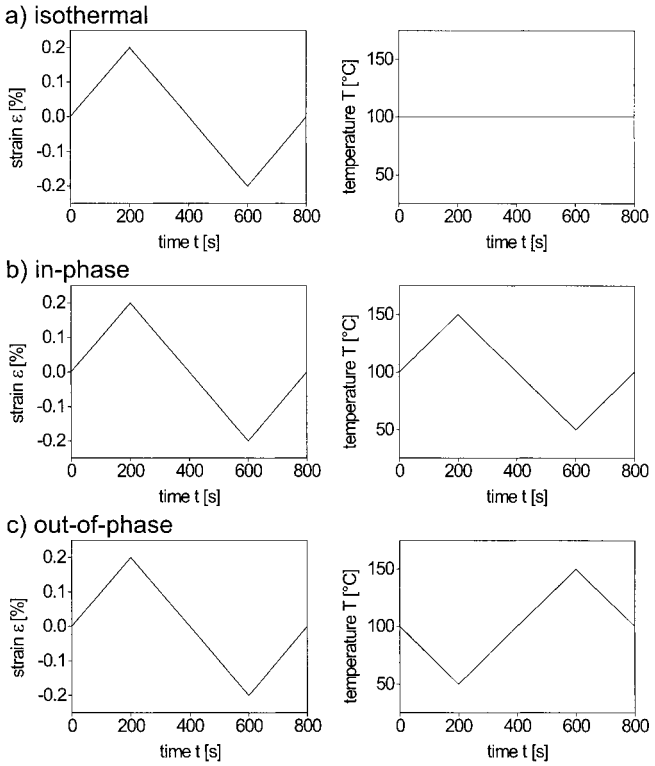

Fig. 8. One cycle of different cyclic thermomechanical loads.

Here it is distinguished when the temperature is kept constant, temperature and external strain are in-phase (i.e. maximum/minimum temperature occurs at the time of maximum/minimum strain) or temperature and strain are completely out of phase (i.e. maximum temperature occurs at the time of minimum strain and vice versa). In all cases, we assume a strain amplitude of 0.2% and a temperature amplitude of 50°C around a mean temperature of 100°C.

Fig. 9 summarises macroscopic stress–strain curves for the first, fifth and 40th cycles, respectively, for the different loadings. It can be distinctly perceived that a superimposition of an in-phase temperature results in lower maximum macroscopic stresses as well as absolute values of minimum macroscopic stress compared to the isothermal condition.

Because both the maximum stress and the absolute value of the minimum stress decrease, the extent of asymmetry is lessened. Furthermore, the narrowed width of the hysteresis loops compared to the isothermal loading results from a poorer inelastic deformation of the metallic matrix. This influence of loading on the inelastic deformation will be examined in particular below.

On the contrary, combining thermal and mechanical loads out-of-phase entails higher maximum macroscopic stresses as well as higher absolute values of minimum macroscopic stresses compared to the isothermal case, whereby the asymmetry of loops is intensified. Moreover, the increase in the width of hysteresis curves is caused by increased inelastic deformation of the matrix.

To examine the influence of loading condition on the inelastic deformation, Fig. 10 compares the inelastic work of deformation per cycle w^{i} normalised by the value of inelastic work on the first cycle of isothermal loading w_0^{i}. In comparison with the isothermal case, superimposed in-phase temperature change results in an accelerated reduction of the inelastic work of deformation in the course of the cycles, whereas a superimposed out-of-phase temperature causes a deceleration of the inelastic work of deformation. Evaluating the peak levels in the first cycle, the inelastic work of deformation for the in-phase loading is only 40% of the corresponding value of the isothermal condition, whereas the out-of-phase loading shows a maximum approximately 2.7 times higher than at constant temperature. With the 40th loading cycle, the in-phase loading shows an inelastic work of deformation of only 20% of the corresponding value of the isothermal reference load. The amount of inelastic work of deformation of the out-of-phase loading is now 3.45 times higher than in the reference case. These figures show that the in-phase load leads to a lower

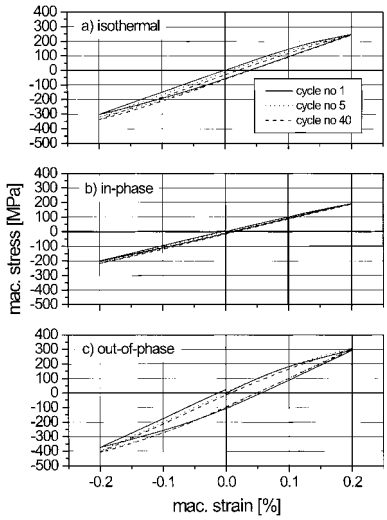

Fig. 9. Stress–strain cycles of the laminate under different temperature–strain phasings.

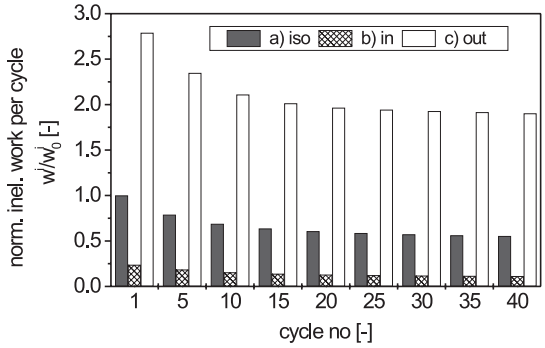

Fig. 10. Normalised inelastic work of deformation per cycle in the process of loading.

inelastic deformation compared to the constant temperature. On the contrary, the out-of-phase loading substantially increases the extent of inelastic deformation.

The difference in the intensity of inelastic straining naturally influences the damage growth in the metallic matrix. Thus, Fig. 11 displays the damage distribution of the two non-isothermal conditions at the end of the 40th cycle with the corresponding graph for the constant temperature already displayed at the bottom of Fig. 7. Under in-phase loading, a maximum value of damage of only 14% of the corresponding maximum at isothermal loading was computed. On the contrary, the out-of-phase loading shows a maximum which is 3.7 times higher than the reference value.

The very different relative distributions attract particular attention. At in-phase load, the highest damaged matrix area resides between adjoining crossed fibres, whereas the relative distribution of the out-of-phase condition is not very different from the isothermal case.

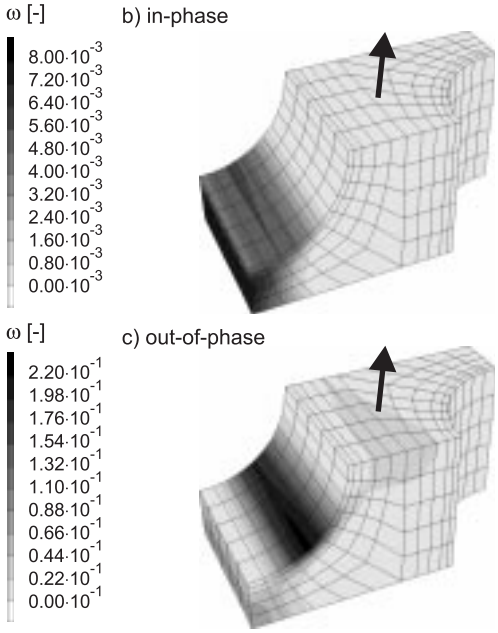

Fig. 11. Damage after 40 cycles of thermomechanical cyclic loading.

Thus, it can be restated that a constant strain amplitude combined with an out-of-phase temperature worsens fatigue lives of the composite compared to the isothermal loading because of increased inelastic deformation and faster damage nucleation and growth. On the contrary, in-phase loading enhances fatigue lives. These results were also experimentally verified by Roush et al. (1994).

6. Conclusion

The current study uses a three-dimensional finite element model to investigate the influence of various mechanical and thermomechanical cyclic loading conditions on the behaviour of cross-ply reinforced aluminium laminates.

Thermal residual stresses induce asymmetric stress–strain hysteresis loops which are characterised by a narrowing in the course of the loading. With increasing external strain amplitudes, the extent of inelastic deformation in the metallic matrix increases significantly, thereby developing damage growth in the metallic matrix. At isothermal load, the damage is highly concentrated in front of the perpendicularly loaded fibre.

Superimposing a cyclic temperature on the top of the mechanical load strongly influences the deformation and damage behaviour of the composite. Thus, an out-of-phase temperature increases the extent of inelastic deformation, in comparison to the isothermal case, promoting damage growth in the metallic matrix. On the contrary, the in-phase condition leads to lower damage values and a damage distribution different from the isothermal load. Therefore, it can be stated that the out-of-phase condition has an adverse effect on the fatigue life of the composite.

Acknowledgements

This research was gratefully supported by the Deutsche Forschungsgemeinschaft (DFG).

References

Aboudi, J., 1982. A continuum theory for fiber-reinforced elastic-viscoplastic composites. International Journal of Engineering Science 20, 605–621.

Bigelow, C.A., 1992. Thermal residual stresses in a silicon-carbide/titanium [0/90] laminate. NASA Technical Memorandum 107649.

Bonora, N., Costanzi, M., Newaz, G., Marchetti, M., 1994. Microdamage effect on the overall response of long fibre/metal-matrix composites. Composites 25 (7), 575–582.

Chaboche, J.L., 1977. Viscoplastic constitutive equations for the description of cyclic and anisotropic behaviour of metals. Bulletin de l'Academie Polonaise de Sciences Sërie des Science Technique 25 (1), 33–42.

Chaboche, J.L., 1988a. Continuum damage mechanics: part I – general concepts. Journal of Applied Mechanics 55, 59–64.

Chaboche, J.L., 1988b. Continuum damage mechanics: part II – damage growth, crack initiation, and crack growth. Journal of Applied Mechanics 55, 65–72.

Dvorak, G.J., Bahei-El-Din, Y.A., 1982. Plasticity analysis of fibrous composites. Journal of Applied Mechanics 49, 327–335.

Flom, Y., Arsenault, R.J., 1986. Deformation of SiC/Al composites. Journal of Metals 38, 31–34.

Fries, V., Ismar, H., Penth, M., 1997. Inelastic deformation behaviour of AlMgSi1. Mechanics Research Communications 24 (4), 359–370.

Hansen, N.R., Schreyer, H.L., 1995. Damage deactivation. Journal of Applied Mechanics 62, 450–458.

Ismar, H., Schmitt, J., 1990. Zur zyklischen Belastung einer Aluminiumlegierung im Bereich kleiner plastischer Formänderungen. Zeitschrift für Angewandte Mathematik und Mechanik 70, T324–T327.

Ismar, H., Penth, M., 1998. Comportement inélastique de l'alliage AlMgSi1 avec prise en compte des effects liés au chargement et à la restauration dépendant du temps. European Physical Journal Applied Physics 2, 27–34.

Ismar, H., Schröter, F., 1999. Modelling and numerical simulation of the thermomechanical behavior of a cross-ply MMC. Computational Materials Science 16, 259–266.

Kachanov, L.M., 1958. Time of the rupture process under creep conditions. Izv Akad Nauk S.S.R. Otd. Tekh Nauk 8, 26–31.
Lemaitre, J., 1985. A continuous damage mechanics model for ductile fracture. Journal of Engineering Materials and Technology 107, 83–89.
Lemaitre, J., 1992. A course on damage mechanics, Springer, Berlin.
Lion, A., 1994. Materialeigenschaften der Viskoplastizität, Ph.D-Thesis, Universität-Gesamthochschule Kassel, Germany.
Mahrenholtz, O., Ismar, H., 1979. Ein Modell des elastisch-plastischen Übergangsverhaltens metallischer Werkstoffe. Abhandlungen der Braunschweiger Wissenschaftlichen Gesellschaft 30, 138–144.
Mall, S., Schubbe, J.J., 1994. Thermo-mechanical fatigue behavior of a cross ply SCS-6/Ti-15–3 metal matrix composite. Composites Science and Technology 50, 49–57.
McClintock, F.A., 1968. A criterion for ductile fracture by growth of holes. Journal of Applied Mechanics 35, 363–371.
Nicholas, T., Kroupa, J.L., Neu, R.W., 1993. Analysis of a [0°/90°] metal-matrix composite under thermomechanical fatigue loading. Composites Engineering 3 (7–8), 675–689.
Rice, J.R., Tracey, D.M., 1969. On the ductile enlargement of voids in triaxial stress fields. Journal of Mechanics and Physics of Solids 17, 201–217.
Roush, J.T., Mall, S., Vaught, W.H., 1994. Thermo-mechanical fatigue behavior of an angle-ply SCS-6/Ti-15-3 metal-matrix composite. Composites Science and Technology 52, 47–59.
Sherwood, J.A., Quimby, H.M., 1995. Micromechanical modeling of damage growth in titanium based metal-matrix composites. Computers and Structures 56 (2/3), 505–514.